Challenges and Issues of Modern Science
2026, Vol. 5, No. 1, ID 342
ISSN: 3083-5704
URL: https://cims.fti.dp.ua/j/article/view/342
DOI: https://doi.org/10.15421/cims.5.342

UDC 621.57:662.99:697

Heat Recovery and Desiccant Wheel Effect on Energy Saving of a Solar Cooling System

Christian Chikezie Aka, Thomas Okechukwu Onah, Barnabas Uchenna Ugwuanyi

Purpose. This paper investigates the integration of a desiccant wheel into a conventional solar cooling system and the feasibility of recovering the heat rejected by the absorption chiller to regenerate the desiccant wheel, thereby improving overall system energy efficiency. **Findings.** The proposed system achieves solar energy savings of 18–31.5% compared to a conventional solar cooling system, depending on operating conditions. **Design /Method / Approach.** Mathematical models for each major component—evacuated tube solar collectors, single-stage and half-effect NH_3–H_2O absorption chillers, and a silica-gel desiccant wheel—were developed and validated against experimental data. A parametric analysis was conducted to evaluate the effects of ambient temperature, relative humidity, fresh air fraction, and regeneration temperature on system performance. **Theoretical Implications.** The study demonstrates that the simultaneous use of absorption and adsorption thermodynamic cycles, coupled through heat recovery, provides a theoretically grounded pathway to improving the coefficient of performance of solar-driven air conditioning systems. **Practical Implications.** The findings offer HVAC engineers and building designers a validated configuration for reducing solar collector area and energy consumption in solar cooling installations, particularly in hot-humid climates such as subtropical Australia. **Originality / Value.** Unlike previous studies that treat absorption cooling and desiccant dehumidification as independent subsystems, this work is among the first to propose recovering the absorption chiller's rejected heat specifically for desiccant regeneration, creating a synergistic coupling that eliminates a dedicated regeneration heat source. **Research Limitations / Future Research.** The study is based on steady-state simulation models; experimental validation of the integrated system and transient performance analysis remain as future work. Economic and life-cycle cost analyses were not included. **Article Type.** Applied Research.

Keywords:

ammonia-water absorption, silica gel, energy efficiency, solar energy, hot-humid climate, air conditioning

---

Мета. Дослідження присвячено інтеграції десикантного колеса у традиційну сонячну охолоджувальну систему та оцінці доцільності використання теплоти відведення абсорбційної холодильної машини для його регенерації з метою підвищення загальної енергетичної ефективності системи. **Результати**. Запропонована система забезпечує економію сонячної енергії на 18–31,5% порівняно з традиційною сонячною охолоджувальною системою залежно від умов експлуатації. **Дизайн / Метод / Підхід**. Математичні моделі ключових компонентів системи — сонячних колекторів, абсорбційних холодильних машин NH_3–H_2O та силікагелевого десикантного колеса — верифіковано на основі експериментальних даних. Параметричний аналіз охопив вплив температури, вологості, частки свіжого повітря та температури регенерації на ефективність системи. **Теоретичне значення**. Поєднання абсорбційного та адсорбційного циклів через рекуперацію теплоти забезпечує обґрунтований шлях до підвищення коефіцієнта продуктивності сонячних систем кондиціювання повітря. **Практичне значення**. Отримані результати надають інженерам HVAC та проєктувальникам будівель апробовану конфігурацію для скорочення площі сонячних колекторів та енергоспоживання в установках сонячного охолодження, зокрема у вологому субтропічному кліматі. **Оригінальність / Цінність**. На відміну від попередніх досліджень, у яких абсорбційне охолодження та десикантне осушення розглядаються як незалежні підсистеми, ця робота є однією з перших, де запропоновано рекуперацію теплоти відведення абсорбційної холодильної машини безпосередньо для регенерації десикантного колеса, що створює синергетичний зв'язок і виключає необхідність у виділеному джерелі теплоти для регенерації. **Обмеження дослідження / Майбутні дослідження**. Дослідження базується на моделях усталеного режиму; експериментальне підтвердження інтегрованої системи та аналіз перехідних процесів залишаються завданнями майбутніх досліджень. Економічний аналіз та оцінка життєвого циклу не включені. **Тип статті**: Прикладне дослідження.

Ключові слова:

аміачно-водна абсорбція, силікагель, енергоефективність, сонячна енергія, вологий субтропічний клімат, кондиціювання повітря

Contributor Details:

Christian Chikezie Aka, Ph.D., Lect. I, Enugu State University of Science and Technology: Enugu, NG, chikezie.aka@esut.edu.ng
Thomas Okechukwu Onah, Assoc. Prof., Enugu State University of Science and Technology: Enugu, NG, Okechukwu.onah@esut.edu.ng
Barnabas Uchenna Ugwuanyi, Ph.D., Lect. I, Federal University of Allied Health Sciences, Enugu: Enugu, NG, ugwuanyiuchenna17@gmail.com

Received: 2026-04-17 *Revised: 2026-05-12* *Accepted: 2026-05-14* *Published: 2026-06-28*

Air conditioning systems have been used for decades to improve human comfort in public buildings, offices, and residential dwellings. Despite continuous improvements in energy efficiency, these systems still require substantial amounts of electrical power. In many regions, the electricity used for air conditioning is generated from fossil fuels, contributing significantly to greenhouse gas emissions. The International Energy Agency (IEA) projects that by 2050, energy demand for space cooling will triple, making it one of the fastest-growing end uses globally (International Energy Agency, 2023; González-Torres et al., 2022). The main aim of this study is to quantify the energy-saving potential of integrating a silica-gel desiccant wheel with a solar-driven NH_3–H_2O absorption chiller in which the heat rejected by the chiller is recovered for desiccant regeneration, and to identify the operating conditions that maximize solar and annual energy savings.

Solar cooling systems represent a promising alternative to conventional electrically driven air conditioning, as they utilize solar thermal energy — a resource that is abundantly available during peak cooling demand periods. The most mature solar cooling technology involves coupling evacuated tube solar collectors with thermally driven absorption chillers (Sheikhani et al., 2018; Al-Falahi et al., 2020). In such systems, hot water produced by the solar collectors is used to drive the absorption cycle, replacing the mechanical compressor of conventional systems with a thermochemical process that requires minimal electricity.

Figure 1 illustrates the fundamental thermodynamic principle underlying all cooling systems: heat Q_2 is extracted from a cold source at temperature T_2 (the conditioned space) using an external energy input W and is rejected to a hot reservoir at temperature T_1 (the environment). For a vapor compression chiller, W represents electrical work supplied to the compressor; for an absorption chiller, W is replaced by thermal energy Qgen supplied to the generator. The total heat rejected to the environment is $Q_1 = Q_2 + W$, which is significantly larger in absorption systems ($Q_1 \approx 1.5$–$1.7\ Q_2$) than in vapor compression systems ($Q_1 \approx 1.2$–$1.3\ Q_2$). This excess rejected heat forms the basis of the heat recovery strategy proposed in this study.

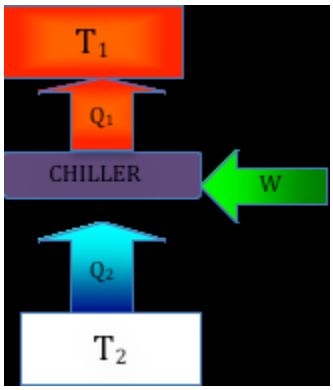

Figure 1 – Generic flow diagram for a chiller system (Source: Authors)

While solar absorption cooling has been demonstrated in numerous pilot installations worldwide (Allouhi et al., 2015; Aka et al., 2024), several technical challenges remain that limit widespread adoption. First, the coefficient of performance (COP) of single-effect absorption chillers typically ranges from 0.5 to 0.7, which is considerably lower than that of conventional vapor compression systems (COP of 3–5). This low COP means that a large solar collector area is required, increasing capital costs. Second, and more critically, the amount of heat rejected by an absorption chiller is substantially higher than that rejected by a vapor compression chiller of equivalent cooling capacity. In a conventional solar cooling installation, this rejected heat is simply dissipated to the environment through a cooling tower or air-cooled condenser, representing a significant waste of thermal energy (Fong et al., 2010).

A third challenge relates to how conventional systems handle the air conditioning load. In a standard air handling unit (AHU), a single cooling coil is responsible for removing both sensible heat (temperature reduction) and latent heat (dehumidification) from the supply air. This combined treatment is inherently inefficient: the air must be cooled below its dew point temperature to condense moisture and then reheated to the desired supply temperature — a process that wastes energy. This problem is exacerbated in subtropical and tropical climates, where the latent heat load represents a significant fraction of the total cooling load.

Figure 2 shows a conventional vapor compression refrigeration cycle. The cycle comprises four main components: (1) the compressor, which raises the pressure and temperature of the refrigerant vapor using electrical work W_c; (2) the condenser, where the high-pressure vapor releases heat Q_{cond} to the environment and condenses to a liquid; (3) the expansion device (throttling valve), which reduces the pressure and temperature of the liquid refrigerant; and (4) the evaporator, where the low-pressure refrigerant absorbs heat Q_{evap} from the conditioned space, producing the cooling effect. This figure serves as the baseline reference for comparing the higher heat rejection of the absorption chiller in this study.

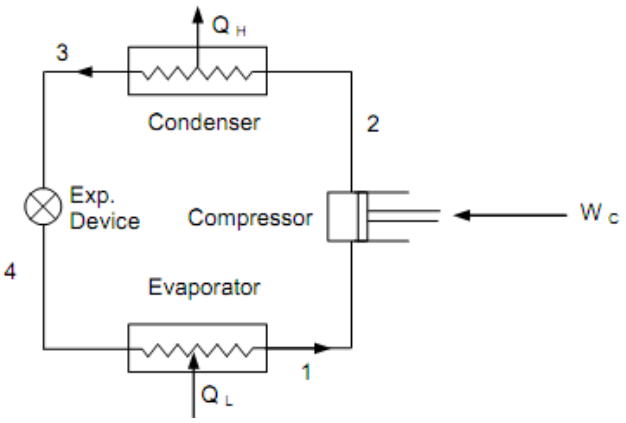

Figure 2 – Schematic of a conventional vapor compression refrigeration system (Source: Authors)

Figure 3(a) shows a temperature–entropy (T–s) diagram illustrating the four processes: isentropic compression (1→2), where the refrigerant temperature rises from the evaporator level to the condenser level; isobaric condensation (2→3), where the superheated vapor releases heat and condenses; isenthalpic throttling (3→4), where the pressure drops and the refrigerant partially evaporates; and isobaric evaporation (4→1), where the remaining liquid absorbs heat from the cooled space.

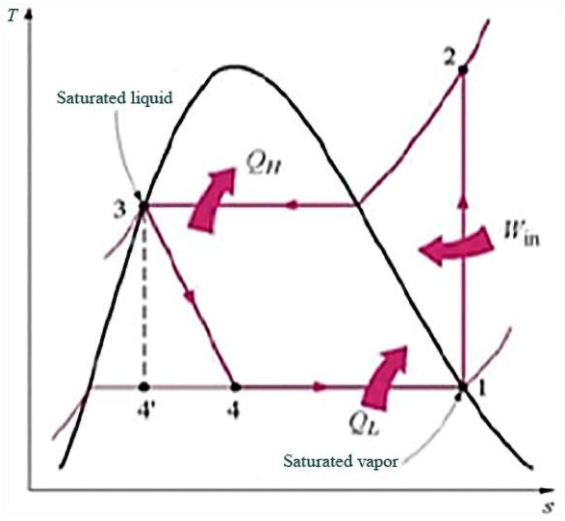

Figure 3(a) –Thermodynamic representation of the vapor compression refrigeration cycle: Temperature–entropy (T–s) diagram (Source: Authors)

Figure 3(b) shows the pressure–enthalpy (p–h) diagram of the same cycle. The area enclosed by the cycle on the T–s diagram (Fig. 3(a)) represents the net work input, while the width of the evaporation process on the p–h diagram corresponds to the cooling capacity Q_{evap}. These diagrams are essential for understanding the thermodynamic limitations that result in the low COP of absorption systems and the consequent large heat rejection that the proposed system seeks to recover.

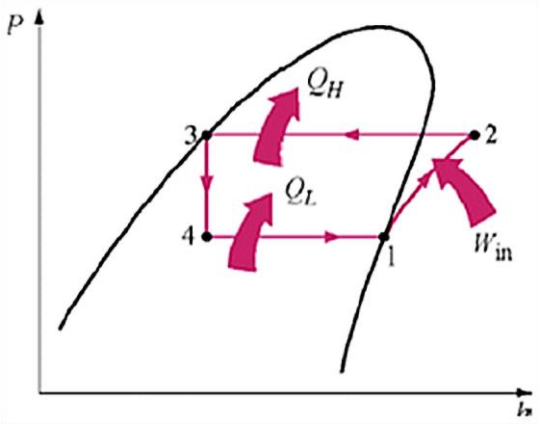

Figure 3(b) – Thermodynamic representation of the vapor compression refrigeration cycle: Pressure–enthalpy (p–h) diagram (Source: Authors)

Desiccant wheels offer an alternative approach to humidity control. These rotating devices use hygroscopic materials — such as silica gel, lithium chloride, or zeolites — to adsorb moisture directly from the air stream without requiring cooling below the dew point (Abdelgaied et al., 2023). After adsorbing moisture in the process section, the desiccant material is regenerated by passing hot air through the regeneration section, typically at temperatures between 60 and 90 °C (Pesaran & Mills, 1987). Desiccant cooling systems have been shown to reduce electricity consumption by 35–50% compared to conventional systems in humidity-dominated climates (Lee & Lee, 2013).

Despite the complementary nature of absorption chillers and desiccant wheels — the former handling sensible cooling and the latter handling latent loads — very few studies have investigated the integration of these two technologies within a single solar cooling system. Moreover, no study identified in the literature has explored the possibility of recovering the heat rejected by the absorption chiller to provide the thermal energy needed for desiccant regeneration, thereby creating a synergistic coupling between the two subsystems.

Literature review

Solar absorption cooling systems

Solar absorption cooling systems have been extensively studied over the past three decades (Herold et al., 2016; Alobaid et al., 2017; Sheikhani et al., 2018). Most installations use either lithium bromide–water (LiBr–H_2O) or ammonia–water (NH_3–H_2O) absorption cycles. LiBr–H_2O systems operate at higher COPs (0.6–0.8 for single effect) but are limited to chilled water temperatures above 0 °C and require water cooling of the absorber and condenser (Aman et al., 2014). NH_3–H_2O systems can achieve sub-zero temperatures and allow air-cooled heat rejection, making them suitable for a wider range of applications, though their COPs are typically lower (0.5–0.65) (Solar Next AG, 2008; Kumar et al., 2020).

Evacuated tube solar collectors are the preferred technology for driving single-effect absorption chillers, as they maintain relatively high efficiency at the operating temperatures required (80–120 °C with water cooling, 125–170 °C with air cooling) (Zambolin & Del Col, 2010). Several studies have demonstrated the feasibility of solar-assisted HVAC systems incorporating thermal storage (Ortiz et al., 2010) and solar-powered absorption cooling in office buildings (Eicker & Pietruschka, 2009). Half-effect (or double-lift) absorption chillers have also been investigated as an alternative to single-effect systems (Xu et al., 2014). These chillers operate at lower generator temperatures (60–80 °C), enabling the use of less expensive flat-plate collectors. However, their COP is approximately half that of single-effect systems (0.25–0.35), resulting in a larger required collector area (Arun et al., 2001).

Unlike the vapor compression cycle (Fig. 2), the mechanical compressor is replaced by a thermochemical "thermal compressor" consisting of an absorber, solution pump, generator, and heat exchanger, as shown in Figure 4.

Solar-heated hot water enters the generator, where the refrigerant (NH_3) is boiled out of the strong solution. The refrigerant vapor then condenses in the condenser (rejecting heat Q_{cond}), expands through a throttle valve, and evaporates in the evaporator (producing cooling Q_{evap}). The weak solution returns from the generator to the absorber, where it re-absorbs the refrigerant vapor from the evaporator, rejecting additional heat Q_{abs}. The total heat rejection $Q_{cond} + Q_{abs}$ is approximately 1.5–1.7 times the cooling capacity — this is the waste heat that the proposed system recovers for desiccant regeneration (Pesaran & Mills, 1987).

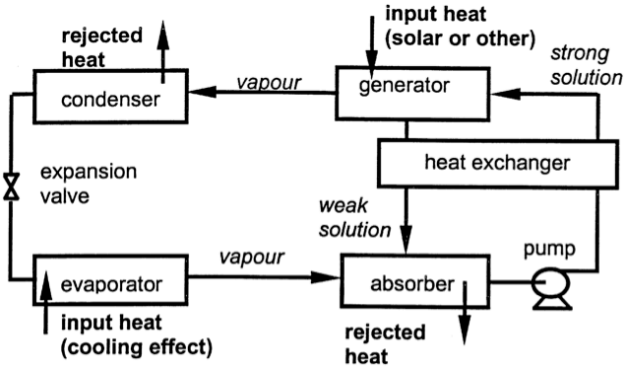

Figure 4 – Flow diagram of a single-effect absorption cycle (Source: Authors)

As shown in Figure 5, the system comprises a generator (where solar heat drives NH_3 out of solution), a rectifier (which removes residual water vapor from the NH_3 stream to prevent ice formation in the evaporator), a condenser, two solution heat exchangers (HX1 and HX2, which improve cycle efficiency by pre-heating the strong solution entering the generator), an evaporator (which produces the chilled water for air conditioning), an absorber, expansion valves, and a solution pump. Hot water from the evacuated tube solar field enters the generator at 90–130 °C; chilled water exits the evaporator at 5–14 °C depending on the operating mode. The numbered state points correspond to the thermodynamic model equations presented in Section 2.

In Figure 6, the dashed lines represent the vapor phase (refrigerant-rich stream from the generator through the condenser, expansion valve, and evaporator); the solid lines represent the liquid phase (solution circuit through the absorber, pump, heat exchangers, and generator). Each numbered point corresponds to a specific thermodynamic state (temperature, pressure, concentration, enthalpy) calculated using the Pátek and Klomfar (1995) correlations. The energy and mass balances at each component (Eqs. 4–6) are formulated using these state-point designations, enabling the calculation of COP, cooling capacity, and — critically — the total heat rejection available for recovery.

Desiccant cooling technology

Desiccant evaporative cooling (DEC) systems have been studied since the 1980s as an alternative to conventional vapor compression air conditioning (ASHRAE, 2016). In a DEC system, a rotating desiccant wheel dehumidifies the process air, which is then cooled by sensible heat exchange and evaporative cooling. The desiccant is regenerated using heated air, which can be provided by solar collectors, waste heat, or gas burners (Venegas et al., 2023).

The performance of a desiccant wheel depends on multiple factors: the desiccant material properties, the wheel geometry (including the regeneration-to-process area ratio), the rotational speed, and the inlet conditions of both process and regeneration air streams (Zhang et al., 2003). Silica gel remains the most widely used desiccant material due to its availability, cost, chemical stability, and effectiveness over a broad range of humidity conditions (Behede et al., 2024).

The wheel is divided into two sectors: the process sector (typically 75% of the wheel face area) and the regeneration sector (25%), as shown in Figure 7. Humid outside air enters the process sector, where moisture is adsorbed onto the silica gel matrix within the honeycomb channels. The air exits this sector at a lower humidity ratio (ω) but at an elevated dry-bulb temperature due to the exothermic heat of adsorption. Simultaneously, hot regeneration air (heated to 60–90 °C) passes through the regeneration sector in the opposite direction, stripping the adsorbed moisture from the

desiccant and restoring its capacity for the next rotation cycle. The wheel rotates at 8–20 revolutions per hour, providing continuous dehumidification. In the proposed system, the regeneration heat is supplied by heat rejected from the absorption chiller rather than by additional solar energy.

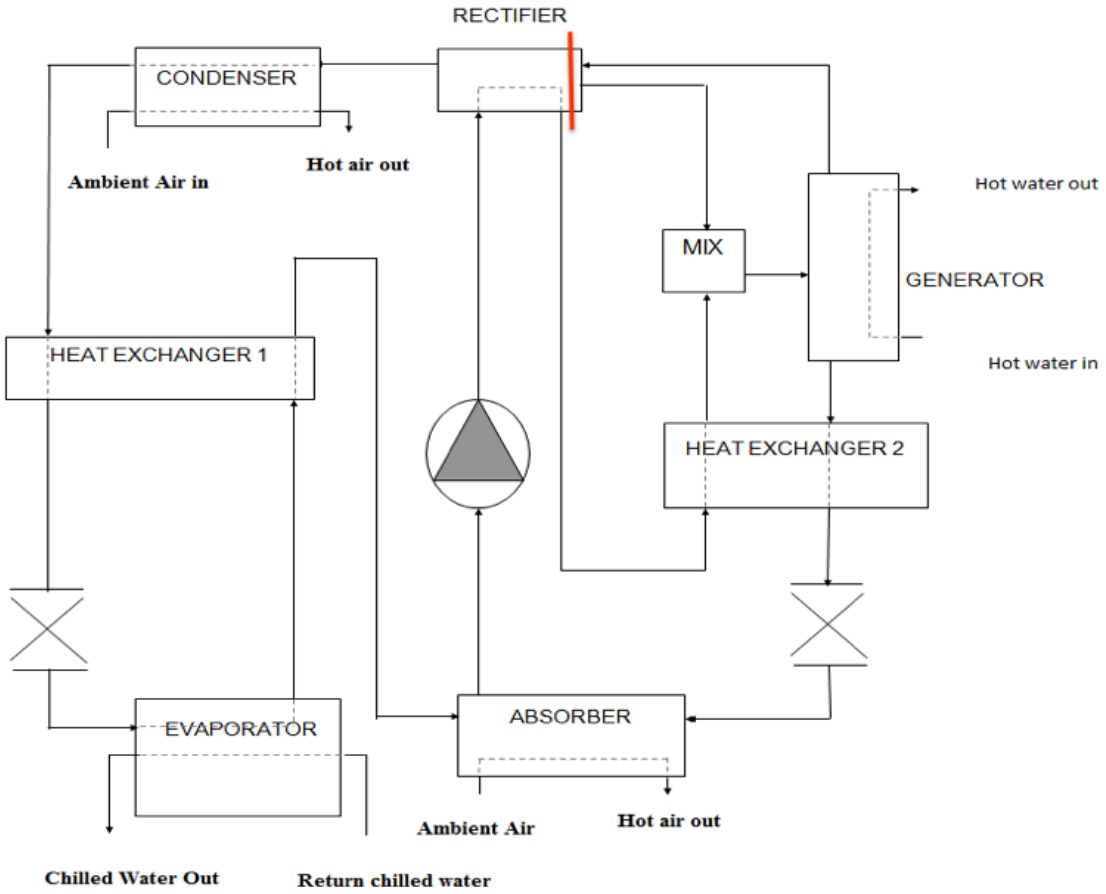

Figure 5 – Detailed schematic of the single-stage NH_3–H_2O absorption chiller used (Source: Authors)

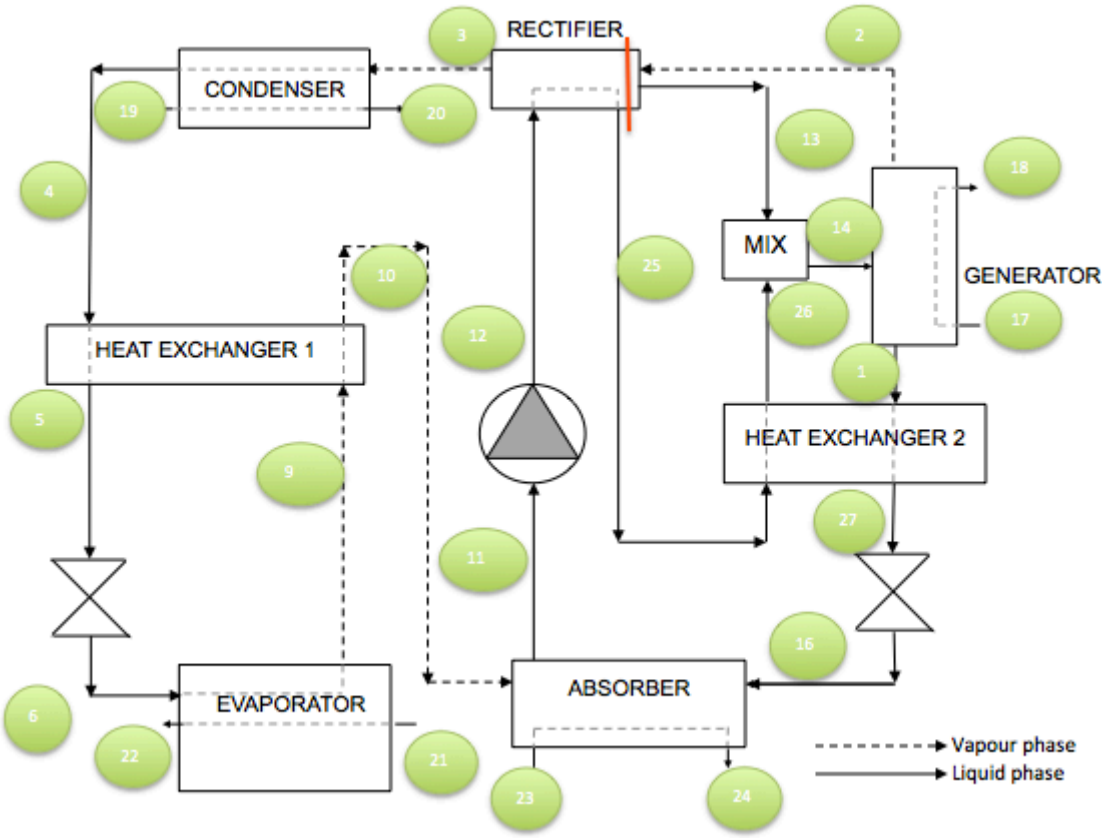

Figure 6 – Numbered state points of the NH_3–H_2O absorption chiller cycle used in the thermodynamic model (Source: Authors)

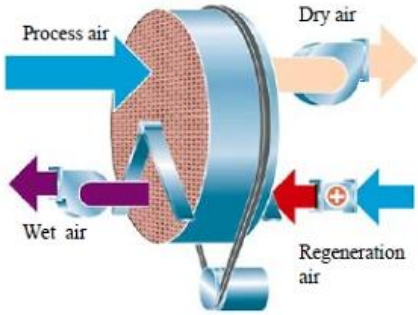

Figure 7 – Cross-sectional view of a typical rotary desiccant wheel (Source: Liu et al., 2022)

In Figure 8, the x-axis represents the relative humidity (φ) at the desiccant surface, and the y-axis represents the equilibrium moisture content (W, kg water per kg dry desiccant). The adsorption branch (lower curve) shows the moisture uptake as relative humidity increases; the desorption branch (upper curve) shows the moisture release during regeneration. The hysteresis between the two curves — greatest at approximately 50% RH — indicates that slightly more energy is required for desorption than is released during adsorption. This isotherm is modeled using the Type 1M equation (Eq. 10) and is critical for predicting the desiccant wheel's dehumidification capacity and the regeneration temperature required. The shape of the isotherm determines the optimal operating range: silica gel performs best when the RH of the process air is between 40% and 80%.

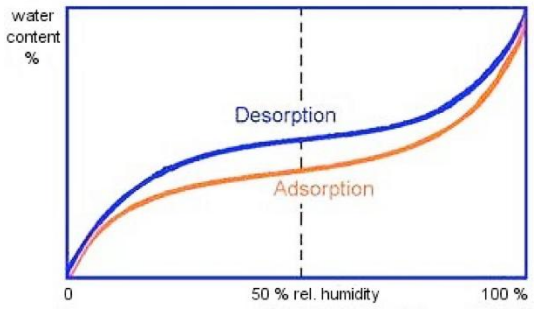

Figure 8 – Adsorption and desorption isotherms for silica gel at 25 °C (Source: Authors)

Hybrid systems combining desiccant wheels with vapor compression chillers have been shown to increase system COP by 20–30% and reduce operating costs by up to 35% compared to conventional systems (Zhang & Niu, 2002; Ge et al., 2010). Hybrid desiccant systems can potentially achieve electrical energy savings of up to 37.5%, attributable to the higher evaporation temperature enabled by pre-dehumidification.

Heat recovery in cooling systems

The desuperheater is a heat exchanger inserted between the compressor discharge and the condenser inlet as shown in Figure 9. It recovers the superheat energy (the shaded region between states 2 and 2' on the p–h diagram) from the high-temperature, high-pressure refrigerant vapor to produce hot water at 55–65 °C.

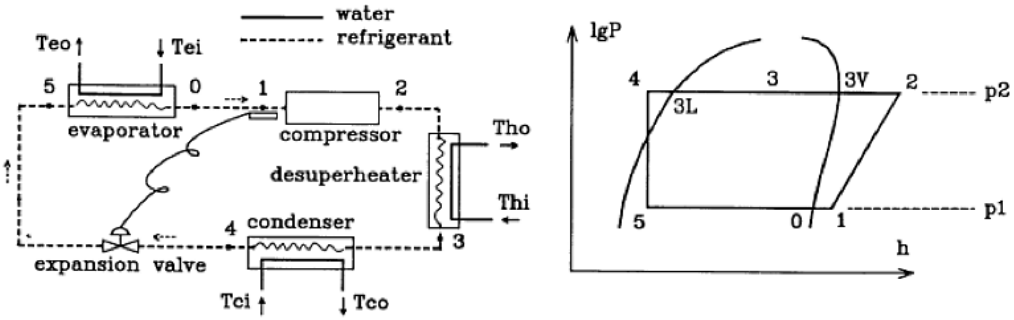

Figure 9 – Vapor compression refrigeration cycle with a desuperheater for heat recovery, shown alongside the corresponding p–h diagram (Source: Behede et al., 2024)

This concept of recovering waste heat from the cooling cycle is analogous to the heat recovery strategy employed in the proposed system; however, in the absorption chiller, the available waste heat is 30–50% greater in magnitude and is available at both the condenser (Q_{cond}) and absorber (Q_{abs}), providing a significantly larger thermal resource for desiccant regeneration.

Heat recovery from the condenser of vapor compression chillers is a well-established practice (Dossat & Horan, 2002; Gordon & Ng, 2000). In absorption chillers, the quantity of heat available for recovery is even greater, as the total heat rejection ($Q_{cond} + Q_{abs}$) is approximately 1.5–1.7 times the cooling capacity, compared to approximately 1.2–1.3 times for vapor compression systems (Gordon & Ng, 2000). Despite this larger quantity of available waste heat, the temperatures at which it is rejected are lower (typically 30–45 °C for water-cooled systems and 35–55 °C for air-cooled systems). However, these temperatures approach the range suitable for desiccant regeneration, particularly for silica gel wheels, which can achieve effective dehumidification with regeneration temperatures as low as 60 °C (Kodama et al., 2005; Abdelgaied et al., 2023).

System description

Conventional solar cooling system (baseline)

The conventional (baseline) solar cooling system consists of three main subsystems: (1) a solar thermal field of evacuated tube collectors that produces hot water; (2) an NH_3–H_2O single-stage absorption chiller that produces chilled water; and (3) an air handling unit (AHU) with a single cooling coil that uses the chilled water to cool and dehumidify the supply air. In this configuration, the cooling coil must handle both the sensible and latent heat loads simultaneously. The heat rejected by the absorption chiller is dissipated to the environment via air-cooled heat exchangers, as shown in Figure 10.

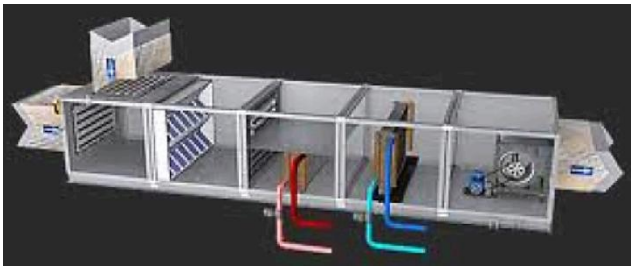

Figure 10 – Standard chamber Air Handling Unit (AHU) used in the conventional solar cooling system (baseline configuration) (Source: Authors)

The unit consists of an intake section where outdoor fresh air is mixed with recirculated return air, a filter section for particulate removal, a cooling coil supplied with chilled water from the absorption chiller, and a supply fan that delivers conditioned air to the occupied space, as depicted in Figure 10. In this conventional arrangement, the single cooling coil must simultaneously reduce the air temperature (sensible cooling) and condense moisture from the air stream (latent cooling). To achieve dehumidification, the coil surface temperature must be maintained below the dew point of the

entering air (typically 10–12 °C), which forces the chiller to produce chilled water at 5–7 °C — a condition that reduces the absorption chiller's COP. This inherent inefficiency motivates the proposed system's approach of separating sensible and latent loads.

The outside air coil handles the full latent load (dehumidification) by cooling fresh air below its dew point, while the return air coil handles the sensible load (temperature control) of the recirculated air. The configuration depicted in Figure 11, while more efficient than the single-coil arrangement (Fig. 10), still requires energy-intensive dew-point cooling for dehumidification.

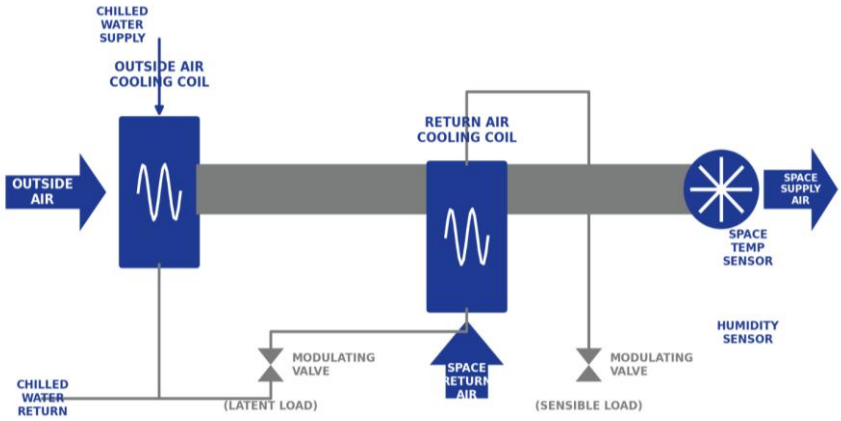

Figure 11 – Schematic of a dual-coil air conditioning system with separate treatment of outside and return air streams (Source: Authors)

The proposed system in this study replaces the outside-air cooling coil with a desiccant wheel, eliminating the need to cool air below its dew point and enabling the use of recovered waste heat for moisture removal instead of valuable solar-generated chilled water.

Proposed integrated system

The proposed system modifies the conventional configuration by adding two components to the AHU: a desiccant wheel and a sensible heat recovery wheel. The outside air first passes through the desiccant wheel, where moisture is adsorbed by the silica gel matrix. The hot, dry air then passes through the sensible heat recovery wheel, where it is pre-cooled by exchanging heat with the exhaust air. Finally, the air passes through the cooling coil, where the remaining sensible heat is removed.

The key innovation is the heat recovery loop connecting the absorption chiller to the desiccant wheel. A portion of the heat rejected at the condenser and absorber is captured by a water circuit and directed to a heating coil in the regeneration air stream of the desiccant wheel. This recovered heat raises the regeneration air temperature to the level required for desorption (typically 60–90 °C). By recovering waste heat for desiccant regeneration, the system eliminates the need for additional solar energy for the regeneration process.

The wheel shown in Figure 12 consists of a cylindrical aluminum matrix that rotates slowly (10–20 rpm) between the supply and exhaust air streams.

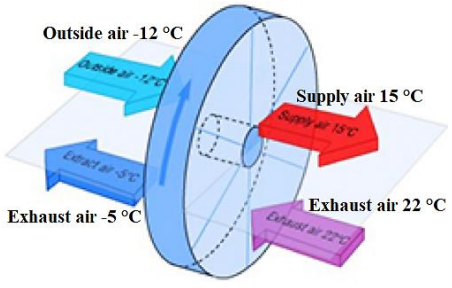

Figure 12 – Rotating sensible heat recovery wheel, also known as a thermal wheel or rotary heat exchanger (Source: Authors)

In the proposed system, this component serves a specific purpose: the process air exiting the desiccant wheel (Fig. 7) is hot (elevated by 10–15 °C due to the heat of adsorption) but dry. The heat recovery wheel transfers heat from this hot process air to the cooler exhaust air stream, pre-cooling the dehumidified supply air before it reaches the cooling coil. This pre-cooling step reduces the sensible cooling load on the absorption chiller by up to 40%, further improving system efficiency. The wheel achieves a sensible heat recovery effectiveness of approximately 75–80%.

Mathematical modelling

Solar collector model

The performance of the evacuated tube solar collectors is modelled using the quasi-steady-state efficiency equation specified in EN 12975-2:2006 (CEN, 2006):

$$\eta = c^0 - c^1 \cdot T^* - c^2 \cdot G \cdot T^{*2}, \quad (1)$$

where η is the instantaneous collector efficiency, c_0 is the optical efficiency (zero-loss coefficient), c_1 and c_2 are the first-order and second-order heat loss coefficients respectively, G is the global solar irradiance on the collector plane (W/m²), and T* is the reduced temperature difference:

$$T^* = \frac{(Tm - Ta)}{G}, \quad (2)$$

where T_m is the mean fluid temperature in the collector and Ta is the ambient air temperature. For the Thermomax DF 100 evacuated tube collectors used in this study, $c_0 = 0.80$, $c_1 = 1.53$ W/(m²·K), and $c_2 = 0.0096$ W/(m²·K²) (ISFH, 2006). The useful heat gain is:

$$Q_{solar} = \eta \cdot A_c \cdot G, \quad (3)$$

where A_c is the total collector aperture area.

Absorption chiller model

The single-stage absorption chiller model is based on mass and energy balances for each component, using the correlations of Pátek and Klomfar (1995) for NH_3–H_2O mixture properties. For the generator:

$$Q_{gen} = \dot{m}_2 h_2 + \dot{m}_1 h_1 - \dot{m}_{14} h_{14}. \quad (4)$$

The COP is:

$$COP = \frac{Q_{evap}}{(Q_{gen} + W_{pump})}. \quad (5)$$

The heat rejected and available for recovery:

$$Q_{reject} = Q_{cond} + Q_{abs} = Q_{gen} + Q_{evap} + W_{pump}. \quad (6)$$

For system-level simulations, chiller performance was modelled using direct interpolation of measured performance data for a Solar Next AG chillii® PSC12 water-cooled single-stage absorption chiller (rated cooling capacity 12 kW, hot water 85/78 °C, chilled water 12/6 °C, cooling water 24/29 °C) (Kumar et al., 2020).

$$COP = f(T_{gen}, T_{cw}, T_{cool}). \quad (7)$$

The COP was computed point-by-point from the manufacturer's test data by varying the generator, evaporator, and cooling-water temperatures over the operating envelope. T_{gen} = 80–130 °C, T_{cw} = 5–15 °C, and T_{cool} = 25–40 °C, achieving $R^2 = 0.987$.

Desiccant wheel model

The desiccant wheel is modelled using the analogy method based on coupled heat and mass transfer equations Ge et al. (2011), assuming a linear driving force approximation and Lewis number of unity (Le = 1). The outlet conditions are determined by effectiveness parameters:

$$\eta_T = \frac{(T_{p,in} - T_{p,out})}{(T_{p,in} - T_{r,in})}, \quad (8)$$

$$\eta_\omega = \frac{(\omega_{p,in} - \omega_{p,out})}{(\omega_{p,in} - \omega_{r,in})}, \quad (9)$$

where subscripts p and r denote process and regeneration sides. The silica gel equilibrium moisture content follows the Type 1M isotherm (Ge et al., 2011):

$$W = W_{max} \cdot \frac{\varphi}{\left(\varphi + (1-\varphi) \cdot exp\left(-\frac{\Delta h_s}{RT}\right)\right)}. \quad (10)$$

Heat recovery model

The heat recovered from the absorption chiller for desiccant regeneration is modelled using the ε-NTU method for a counter-flow heat exchanger:

$$Q_{rec} = \varepsilon \cdot C_{min} \cdot \left(T_{reject,in} - T_{reg,air,in}\right), \quad (11)$$

where ε is the heat exchanger effectiveness (assumed 0.75). The regeneration air temperature after the heat recovery coil is:

$$T_{reg} = T_{reg,air,in} + \frac{Q_{rec}}{(\dot{m}_{air} \cdot c_{p,air})}. \quad (12)$$

When the recovered heat is insufficient, supplementary solar heat is drawn from the solar field.

Cooling coil model

The cooling coil is modeled using the ε-NTU method for a cross-flow heat exchanger. In the proposed system, the coil handles only the sensible heat load; in the conventional system, it handles both sensible and latent loads:

$$Q_{coil} = \dot{m}_{air} \cdot \left(h_{air,in} - h_{air,out}\right) \quad (13)$$

Model validation

The solar collector model was validated against EN 12975-2 test report data for the Thermomax DF 100 evacuated tube collector (Aka et al., 2024), achieving agreement within +0.73% to −2.91%. The absorption chiller COP was computed directly from measured data for the Solar Next AG chillii® PSC12 (Kumar et al., 2020), eliminating curve-fitting errors and the need for a separate error metric. The desiccant wheel model was validated against the experimental data of Ge et al. (2011) for a silica gel wheel operating at regeneration temperatures of 60–100 °C; the predicted outlet humidity ratios agreed within ±8%.

Results and discussion

Effect of ambient temperature

The influence of ambient temperature on solar energy savings was evaluated at a fixed relative humidity of 60% and a fresh air fraction of 30%. The data are presented in Table 1.

Table 1 – Effect of ambient temperature on system performance at RH = 60% and fresh air fraction = 30% (Source: Authors)

T_{amb} (°C)	$Q_{cooling,conv}$ (kW)	$Q_{cooling,prop}$ (kW)	COP_{conv}	COP_{prop}	Solar saving (%)
28	7.2	7.2	0.52	0.58	18.2
30	8.5	8.5	0.54	0.60	21.0
32	9.8	9.8	0.55	0.62	23.5
35	11.8	11.8	0.53	0.61	27.3
38	13.5	13.5	0.50	0.59	31.5

Table 1 presents the effect of ambient temperature on system performance. Both systems deliver identical cooling outputs ($Q_{cooling}$), confirming that the proposed system meets the same thermal comfort requirements. As ambient temperature increases from 28 °C to 38 °C, solar energy savings rise from 18.2% to 31.5%. This increasing trend occurs because higher ambient temperatures produce higher latent loads (at constant RH), which the desiccant wheel handles effectively using recovered heat rather than solar-generated chilled water. The conventional system's COP decreases at higher ambient temperatures (due to higher condensing temperatures), while the proposed system maintains a higher COP because the chiller handles only the sensible load and operates at elevated chilled water temperatures. The improvement in COP from 0.50 to 0.59 at 38 °C represents an 18% enhancement, directly translating to reduced solar collector area requirements.

In Figure 13, the bar chart (right axis) shows that solar savings increase nearly linearly from 18.2% at 28 °C to 31.5% at 38 °C, driven by the growing latent load fraction at higher temperatures.

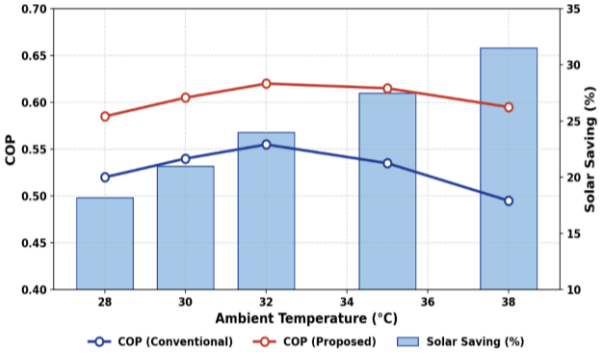

Figure 13 – Effect of ambient temperature on COP and solar energy saving (Source: Authors)

The line plots (left axis) reveal a widening gap between the proposed and conventional system COPs, as the proposed system's chiller benefits from operating at higher chilled water temperatures while the conventional system's COP degrades due to elevated condensing temperatures. The crossover at 35 °C — where the conventional COP begins falling while the proposed COP remains stable — highlights the proposed system's resilience to extreme heat conditions.

Effect of relative humidity

The impact of varying relative humidity on system performance was assessed at a constant ambient temperature of 32 °C.

At 40% RH, solar energy savings are a modest 12.5%, as the latent load constitutes a small fraction of the total cooling load and the desiccant wheel provides limited benefit. As relative humidity increases to 80%, savings rise to 28.8%, reflecting the growing latent load fraction. The relationship is approximately linear between 50% and 70% RH, with each 10-percentage-point increase in RH yielding approximately 5 percentage points of additional solar savings. These results confirm that the proposed system offers the greatest advantage in humid subtropical and tropical climates, where latent loads typically represent 30–50% of the total cooling load.

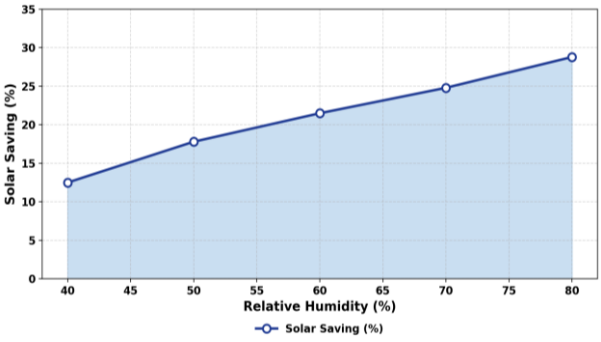

Figure 14 – Effect of relative humidity on solar energy saving at T_{amb} = 32 °C (Source: Authors)

The shaded area chart of Figure 14 illustrates the monotonic increase in solar savings from 12.5% at 40% RH to 28.8% at 80% RH. The relationship is approximately linear between 50% and 70% RH (slope ≈ 0.5% saving per 1% RH increase), reflecting the proportional growth of the latent load fraction.

Above 70% RH, the curve begins to flatten as the desiccant wheel approaches its adsorption capacity at the given regeneration temperature. This graph demonstrates that the proposed system is most advantageous in subtropical and tropical climates (Brisbane design RH ≈ 58%), where latent loads constitute 30–50% of total cooling demand.

Effect of fresh air fraction

The fresh air fraction (ratio of outdoor air to total supply air) directly affects the latent load seen by the desiccant wheel. At a 10% fresh air fraction, savings are modest (8–12%) because most of the air is recirculated and already dehumidified. At 100% fresh air (as in hospitals, laboratories, and some commercial buildings), savings reach 25–35%, as the entire latent load of the outdoor air is handled by the desiccant wheel.

As shown in Figure 15, the bars (right axis) show the latent load increasing linearly with fresh air fraction, as each unit of outdoor air introduces a fixed moisture content. The line plot (left axis) shows solar savings rising sharply from 10% to 23.5% as fresh air fraction increases from 10% to 30%, then more gradually toward 33.8% at 100%. The diminishing returns above 50% occur because the desiccant wheel's dehumidification capacity becomes saturated, requiring supplementary solar heat for regeneration. Buildings with mandatory high ventilation rates (hospitals: 100%, laboratories: 80–100%) would benefit most from this system, achieving 30–34% solar savings.

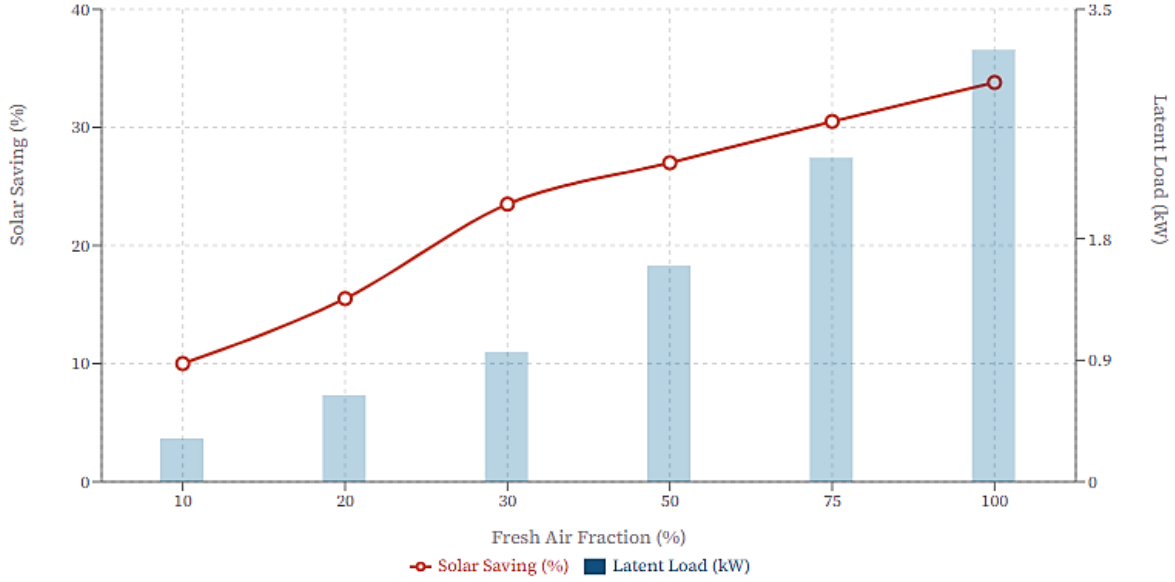

Figure 15 – Effect of fresh air fraction on solar energy saving and latent load at T_{amb} = 32 °C, RH = 60% (Source: Authors)

Effect of regeneration temperature

Table 2 reveals a critical design trade-off in the integrated system. The column Δω represents the humidity ratio reduction achieved by the desiccant wheel: at a 50 °C regeneration temperature, only 2.1 g/kg of moisture is removed, whereas at 100 °C, 6.8 g/kg is removed — a 3.2-fold improvement.

Table 2 – Effect of regeneration temperature on desiccant wheel performance and system energy saving at T_{amb} = 32 °C, RH = 60% (Source: Authors)

T_{reg} (°C)	$\Delta\omega$ (g/kg)	$COP_{chiller}$	η_{solar} (%)	Solar saving (%)
50	2.1	0.48	58	10.2
60	3.8	0.52	55	18.5
70	5.2	0.55	52	24.8
80	6.0	0.54	48	26.5
90	6.5	0.52	44	25.1
100	6.8	0.49	40	22.3

However, higher regeneration temperatures require the solar collectors to operate at higher fluid temperatures (to provide supplementary heat when the recovered heat is insufficient), which reduces collector efficiency η_{solar} from 58% to 40%. The chiller COP also shows non-monotonic behavior: it initially improves (from 0.48 to 0.55) as the desiccant wheel removes more latent load, allowing the chiller to operate at higher chilled water temperatures, but then decreases above 80 °C as the system approaches thermal limitations. The net result is that overall solar energy savings peak at 70–80 °C, with the optimum at approximately 75 °C. This finding is significant for system design: it establishes that the absorption chiller's rejected heat (typically available at 35–55 °C) must be supplemented by a modest amount of solar heat to reach the optimal 70–80 °C regeneration range.

As depicted in Figure 16, the green bars (right axis) show moisture removal (Δω) increasing with regeneration temperature, from 2.1 g/kg at 50 °C to 6.8 g/kg at 100 °C. The dashed blue line shows collector efficiency declining linearly from 58% to 40% over the same range, as higher operating temperatures increase thermal losses. The red line shows solar energy savings peaking at 26.5% near 75–80 °C (dashed vertical reference line), representing the optimal balance point. Above 80 °C, the marginal gain in dehumidification is outweighed by the loss in collector efficiency and the degradation of chiller COP, resulting in a net decrease in system performance.

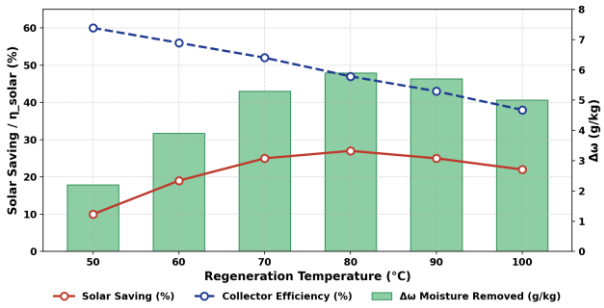

Figure 16 – Regeneration temperature optimization showing the trade-off between dehumidification effectiveness and solar collector efficiency (Source: Author)

Overall system efficiency comparison

The overall system efficiency, combining the solar field, absorption chiller, and desiccant wheel with heat recovery, is:

$$\eta_{sys} = \frac{Q_{cooling}}{(G \cdot A_c)} \quad (14)$$

Table 3 provides a comprehensive side-by-side comparison of all key performance metrics. The solar collector efficiency improves by 4–6% because the proposed system can operate the collectors at a lower mean temperature (the regeneration heat comes from waste heat recovery, reducing the solar field's temperature burden). The chiller COP improves by 5–8% because the chiller handles only

sensible cooling at elevated chilled water temperatures (10–14 °C instead of 5–7 °C). The combined effect produces a system COP improvement of 30–45%. Critically, solar energy requirements drop by 18–32%, meaning the proposed system can either use a smaller collector field for the same cooling output or produce more cooling from the same collector area. The collector area reduction of 15–30% directly translates to capital cost savings, as solar collectors represent 40–50% of the total system cost in solar cooling installations.

Table 3 – Comprehensive comparison of system efficiencies between conventional and proposed solar cooling systems (Source: Authors)

Parameter	Conventional	Proposed	Improvement
Solar collector efficiency	0.50–0.55	0.52–0.58	+4–6%
Chiller COP	0.55–0.60	0.58–0.65	+5–8%
System COP (solar-to-cooling)	0.18–0.25	0.25–0.35	+30–45%
Solar energy required (relative)	1.00	0.68–0.82	−18–32%
Collector area required (relative)	1.00	0.70–0.85	−15–30%

In summary, the parametric analysis and case study results demonstrate that the proposed integrated system consistently outperforms the conventional solar cooling configuration across the investigated range of operating conditions. The findings are consistent with the broader literature on hybrid desiccant-vapor compression systems, which report electricity savings of 20–37.5% (Niu et al., 2002; Ge et al., 2010). The present work extends these findings to solar absorption systems and demonstrates that heat recovery provides an additional efficiency layer not available with vapor compression systems, where rejection temperatures are lower.

Future work should focus on experimental validation, dynamic modeling, including thermal storage effects, and optimization of the heat recovery loop. Advanced desiccant materials (e.g., composite silica gel–lithium chloride) could further enhance performance by 20–50% at equivalent regeneration temperatures (Liu et al., 2022).

Conclusions

This study examined the energy-saving potential of integrating a silica-gel desiccant wheel into a conventional solar-driven absorption cooling system, using the heat rejected by an NH_3–H_2O absorption chiller to regenerate the wheel. Based on the validated component models and the simulated operating scenarios, the following conclusions can be drawn.

1. The proposed configuration achieves instantaneous solar energy savings of 18–31.5% relative to a conventional single-effect solar absorption system. The largest savings are obtained under hot and humid conditions, namely ambient temperatures above 35 °C and relative humidity above 70%, where the latent load dominates.

2. The heat rejected by the NH_3–H_2O chiller is sufficient to partially or fully regenerate the silica-gel wheel within the 60–80 °C range, thereby displacing a corresponding share of the solar thermal demand and reducing the required collector area for a given cooling duty.

3. Decoupling latent and sensible heat removal allows the absorption chiller to operate at higher chilled-water temperatures, increasing its COP by 5–8% and lowering the driving-temperature requirement at the generator.

4. The most favorable performance is obtained for a regeneration temperature of 70–80 °C, a fresh-air fraction of 25–40%, and ambient conditions exceeding 30 °C and 60% RH, which jointly balance dehumidification effectiveness and solar collector efficiency.

5. The concept is well suited to residential, hospitality, and light-commercial buildings in subtropical and tropical climates, particularly those with high ventilation and latent loads.

Scientific contribution. The work provides quantitative evidence that the irreversibilities associated with simultaneous moisture and sensible-heat removal in conventional vapor-compression and single-effect absorption AHUs can be substantially reduced by separating the two processes through a desiccant wheel regenerated by chiller-rejected heat. The validated models of the collector, the NH_3–H_2O chiller (calibrated against measured data from the Solar Next AG chillii® PSC12 unit), and the silica-gel wheel extend the existing solar-cooling literature by characterizing the synergistic coupling between adsorption dehumidification and absorption refrigeration under realistic subtropical boundary conditions.

Practical implications. The results enable HVAC engineers and building designers in hot-humid climates to (i) downsize evacuated-tube collector fields without compromising indoor comfort, (ii) retrofit existing single-effect solar absorption installations by adding a desiccant wheel on the heat-rejection circuit, and (iii) prioritize the deployment of such systems in buildings with high ventilation and latent loads, where the benefit is most pronounced.

Future work. Further research should focus on (i) experimental validation of the fully integrated prototype under transient operation, (ii) dynamic, control-oriented modeling that includes thermal storage and part-load behavior, (iii) life-cycle and techno-economic assessment across different climatic zones, and (iv) the substitution of silica gel by composite or metal–organic-framework sorbents capable of enhancing dehumidification performance within the 60–80 °C regeneration window provided by the chiller heat-rejection loop.

Authorship contribution statement

Christian Chikezie Aka: Conceptualization, Methodology, Software, Validation, Formal analysis, Writing – original draft.

Thomas Okechukwu Onah: Supervision, Data curation, Resources, Writing – review & editing.

Barnabas Uchenna Ugwuanyi: Supervision, Project administration, Investigation, Visualization.

Declaration of Competing Interest

The authors declare that they have no known competing financial interests or personal relationships that could have appeared to influence the work reported in this paper.

Data availability

Data will be made available on request.

References

Abdelgaied, M., Saber, M. A., Bassuoni, M. M., & Khaira, A. M. (2023). Adsorption air conditioning: a comprehensive review in desiccant materials, system progress, and recent studies on different configurations of hybrid solid desiccant air conditioning systems. *Environmental Science and Pollution Research, 30*(11), 28344–28372. https://doi.org/10.1007/s11356-023-25209-z

Aka, C. C., Onah, T. O., & Egwuagu, O. M. (2024). Design modification of elliptical vessel solar receiver by response surface methodology. *Global Journal of Engineering and Technology Advances, 19*(1), 129–142. https://doi.org/10.30574/gjeta.2024.19.1.0064

Al-Falahi, A., Alobaid, F., & Epple, B. (2020). Thermo-Economic Evaluation of Aqua-Ammonia Solar Absorption Air Conditioning System Integrated with Various Collector Types. *Entropy, 22*(10), 1165. https://doi.org/10.3390/e22101165

Allouhi, A., Kousksou, T., Jamil, A., Bruel, P., Mourad, Y., & Zeraouli, Y. (2015). Solar driven cooling systems: An updated review. *Renewable and Sustainable Energy Reviews, 44*, 159–181. https://doi.org/10.1016/j.rser.2014.12.014

Alobaid, M., Hughes, B., Calautit, J. K., O'Connor, D., & Heyes, A. (2017). A review of solar driven absorption cooling with photovoltaic thermal systems. *Renewable and Sustainable Energy Reviews, 76*, 728–742. https://doi.org/10.1016/j.rser.2017.03.081

Aman, J., Ting, D. S.-K., & Henshaw, P. (2014). Residential solar air conditioning: Energy and exergy analyses of an ammonia–water absorption cooling system. *Applied Thermal Engineering, 62*(2), 424–432. https://doi.org/10.1016/j.applthermaleng.2013.10.006

Arun, M. B., Maiya, M. P., & Murthy, S. S. (2001). Performance comparison of double-effect parallel-flow and series flow water–lithium bromide absorption systems. *Applied Thermal Engineering, 21*(12), 1273–1279. https://doi.org/10.1016/s1359-4311(01)00005-9

ASHRAE. (2016). *2016 ASHRAE handbook: HVAC systems and equipment (SI ed.)*. American Society of Heating, Refrigerating and Air-Conditioning Engineers. https://books.google.com/books?id=iwCJAQAACAAJ

Behede, B., Chakrabarti, S., & Wankhede, U. (2024). Development of rotary dehumidifier with silica-gel-based composite desiccant. *Thermal Science, 28*(5 Part B), 4223–4233. https://doi.org/10.2298/tsci231016174b

CEN. (2006). EN 12975-2:2006: *Thermal solar systems and components—Solar collectors—Part 2: Test methods*. European Committee for Standardization. https://shop.standards.ie/en-ie/standards/en-12975-2-2006-331244_saig_cen_cen_761800

Dossat, R. J., & Horan, T. J. (2002). *Principles of refrigeration* (5th ed.). Prentice Hall. https://books.google.com/books?id=EE62QgAACAAJ

Eicker, U., & Pietruschka, D. (2009). Design and performance of solar powered absorption cooling systems in office buildings. *Energy and Buildings, 41*(1), 81–91. https://doi.org/10.1016/j.enbuild.2008.07.015

Fong, K. F., Chow, T. T., Lee, C. K., Lin, Z., & Chan, L. S. (2010). Comparative study of different solar cooling systems for buildings in subtropical city. *Solar Energy, 84*(2), 227–244. https://doi.org/10.1016/j.solener.2009.11.002

Ge, T. S., Dai, Y. J., & Wang, R. Z. (2011). Performance study of silica gel coated fin-tube heat exchanger cooling system based on a developed mathematical model. *Energy Conversion and Management, 52*(6), 2329–2338. https://doi.org/10.1016/j.enconman.2010.12.047

Ge, T. S., Ziegler, F., & Wang, R. Z. (2010). A mathematical model for predicting the performance of a compound desiccant wheel (A model of compound desiccant wheel). *Applied Thermal Engineering, 30*(8-9), 1005–1015. https://doi.org/10.1016/j.applthermaleng.2010.01.012

González-Torres, M., Pérez-Lombard, L., Coronel, J. F., Maestre, I. R., & Yan, D. (2022). A review on buildings energy information: Trends, end-uses, fuels and drivers. *Energy Reports, 8*, 626–637. https://doi.org/10.1016/j.egyr.2021.11.280

Gordon, J. M., & Ng, K. C. (2000*). Cool thermodynamics: The engineering and physics of predictive, diagnostic and optimization methods for cooling systems*. Cambridge International Science Publishing. https://books.google.com/?id=A9yNQgAACAAJ

Herold, K. E., Radermacher, R., & Klein, S. A. (2016). *Absorption chillers and heat pumps* (2nd ed.). CRC press. https://doi.org/10.1201/b19625

International Energy Agency. (2023). *Space cooling: Tracking report*. International Energy Agency https://www.iea.org/reports/space-cooling

ISFH. (2006). Report of performance test according EN 12975-2 for a glazed solar collector (Report No. 107-06/D). Institut für Solarenergieforschung GmbH. https://www.scribd.com/document/868120592

Kodama, A., Watanabe, N., Hirose, T., Goto, M., & Okano, H. (2005). Performance of a Multipass Honeycomb Adsorber Regenerated by a Direct Hot Water Heating. *Adsorption, 11*(S1), 603–608. https://doi.org/10.1007/s10450-005-5992-6

Kumar, A., Said, Z., & Bellos, E. (2020). An up-to-date review on evacuated tube solar collectors. *Journal of Thermal Analysis and Calorimetry, 145*(6), 2873–2889. https://doi.org/10.1007/s10973-020-09953-9

Lee, S. H., & Lee, W. L. (2013). Site verification and modeling of desiccant-based system as an alternative to conventional air-conditioning systems for wet markets. *Energy, 55*, 1076–1083. https://doi.org/10.1016/j.energy.2013.04.029

Liu, S., Jeong, C. H., & Yeo, M. S. (2022). Development and performance analysis of a novel multi-zone hybrid desiccant cooling system. In *CLIMA 2022 conference, 14th REHVA HVAC World Congress*. TU Delft OPEN Publishing, Delft University of Technology. https://doi.org/10.34641/clima.2022.188

Niu, J. L., Zhang, L. Z., & Zuo, H. G. (2002). Energy savings potential of chilled-ceiling combined with desiccant cooling in hot and humid climates. *Energy and Buildings, 34*(5), 487–495. https://doi.org/10.1016/s0378-7788(01)00132-3

Ortiz, M., Barsun, H., He, H., Vorobieff, P., & Mammoli, A. (2010). Modeling of a solar-assisted HVAC system with thermal storage. *Energy and Buildings, 42*(4), 500–509. https://doi.org/10.1016/j.enbuild.2009.10.019

Pátek, J., & Klomfar, J. (1995). Simple functions for fast calculations of selected thermodynamic properties of the ammonia-water system. *International Journal of Refrigeration, 18*(4), 228–234. https://doi.org/10.1016/0140-7007(95)00006-w

Pesaran, A. A., & Mills, A. F. (1987). Moisture transport in silica gel packed beds—I.Theoretical study. International *Journal of Heat and Mass Transfer, 30*(6), 1037–1049. https://doi.org/10.1016/0017-9310(87)90034-2

Sheikhani, H., Barzegarian, R., Heydari, A., Kianifar, A., Kasaeian, A., Gróf, G., & Mahian, O. (2018). A review of solar absorption cooling systems combined with various auxiliary energy devices. *Journal of Thermal Analysis and Calorimetry, 134*(3), 2197–2212. https://doi.org/10.1007/s10973-018-7423-4

Solar Next AG. (2008). *chilli® PSC12 – Absorption chiller*. Solar Next AG. https://solarnext.de

Venegas, T., Qu, M., Wang, L., Liu, X., Gluesenkamp, K., & Gao, Z. (2023). Review of liquid desiccant air dehumidification systems coupled with heat pump: System configurations, component design, and performance. *Energy and Buildings, 279*, 112655. https://doi.org/10.1016/j.enbuild.2022.112655

Xu, Z. Y., & Wang, R. Z. (2014). Experimental verification of the variable effect absorption refrigeration cycle. *Energy, 77*, 703–709. https://doi.org/10.1016/j.energy.2014.09.044

Zambolin, E., & Del Col, D. (2010). Experimental analysis of thermal performance of flat plate and evacuated tube solar collectors in stationary standard and daily conditions. *Solar Energy, 84*(8), 1382–1396. https://doi.org/10.1016/j.solener.2010.04.020

Zhang, L. Z., & Niu, J. L. (2002). Performance comparisons of desiccant wheels for air dehumidification and enthalpy recovery. *Applied Thermal Engineering, 22*(12), 1347–1367. https://doi.org/10.1016/s1359-4311(02)00050-9

Zhang, X. J., Dai, Y. J., & Wang, R. Z. (2003). A simulation study of heat and mass transfer in a honeycombed rotary desiccant dehumidifier. *Applied Thermal Engineering, 23*(8), 989–1003. https://doi.org/10.1016/s1359-4311(03)00047-4